

Transportable Energy Storage Assisted Post-disaster Restoration of Distribution Networks with Renewable Generations

Shihao Zhao^a, Kang Li^{*a}, Mingjia Yin^b, James Yu^c, Zhile Yang^d, Yihuan Li^e

^a*School of Electronic and Electrical Engineering, University of Leeds, Leeds, LS2 9JT, UK (e-mail:k.li1@leeds.ac.uk)*

^b*National Grid ESO, National Grid St Catherine's Lodge, Bearwood Road, Sindlesham RG41 5BN, UK*

^c*Scottish Power Energy Networks, Glasgow G32 8FA, UK*

^d*Shenzhen Institute of Advanced Technology, Chinese Academy of Sciences, Shenzhen, Guangdong, 518055, China*

^e*School of Control and Computer Engineering, North China Electric Power University, Beijing, 102206, China*

Abstract

More frequent extreme weather events due to climate change impose significant challenges on the post-disaster restoration of distribution systems with significant penetration of renewable generations. To address this challenge, this paper investigates a restoration scheme for distribution networks integrated with renewable generations, and transportable energy storage systems moving along a transportation network, such as railway or road network, are used to support the network restoration after the fault event. To achieve this, for given fault conditions, topological reconfiguration is first facilitated via the soft open point (SOP) technology, and local renewable generators and loads are rapidly regrouped to form microgrids for post-disaster restoration. Then, assisted with transportable energy storage, the resources within the microgrids can be dispatched more efficiently, facilitating a more efficient post-disaster recovery process. To enable a cost-effective restoration of the distribution network, an economic model is formulated with the aim of minimizing the economic losses during the post-disaster restoration process. Case studies considering a significant number of failure scenarios show that the proposed transportable energy storage-assisted restoration scheme can effectively minimize costs during the post-disaster period considering various load types across different areas. This scheme not only achieves cost-effective post-disaster restoration but also ensures compliance with the constraints of the electrical networks, achieving up to 93.3% recovery cost reduction and 74.25% increase in critical load restoration.

Nomenclature

	η_b^{ch}	Charging efficiency of TESS b (%)	
DS	Distribution network	η_b^{dis}	Discharging efficiency of TESS b (%)
ESS	Energy storage system	$\gamma_{b,(p,q),t}$	Binary variable, 1 if TESS b transits from station p to station q at time interval t
GHG	Greenhouse gas	\mathbb{B}	The set of TESSs
HILP	High-impact but low-probability	\mathbb{E}	The set of branches of the power system
O&M	Operation and maintenance	\mathbb{P}	The set of reconfiguration topologies
RGs	Renewable generations	\mathbb{Q}	The set of arcs for TESS
SESS	Stationary energy storage system	\mathbb{Q}_p^+	The set of arcs starting from the station p
SOC	State of charge	\mathbb{Q}_p^-	The set of arcs ending at the station q
SOP	Soft open point	\mathbb{S}	The set of buses of the power system
TESS	Transportation energy storage system	\mathbb{T}	The set of time spans
TSN	Time-space network	\mathbb{Y}	The set of all stations of TESS
WC	Wind curtailment	\mathbb{Y}^+	The set of all stations of real stations of TESS
WTG	Wind turbine generator	ρ^{g2m}	Sell price of the electricity from the main grid to the microgrids (\$/kWh)
$\delta_{b,p,t}$	Binary variable, 1 if TESS b locates at station p at time interval t		

ρ^{m2c}	Sell price of the electricity from the microgrids to the customers (\$/kWh)
ρ^{WC}	The price of wind curtailment (\$/kWh)
$\varphi_{b,t}^{ch}, \varphi_{b,t}^{ch}$	Binary variable, 1 if TESS b is charging/discharging at time interval t
b	Index of TESS
C^{INT}	Interruption cost of the loads which can not be fed (\$)
C^{OM}	O&M cost of all WGTs and TESSs (\$)
C^{POS}	Transportation cost of TESSs (\$)
C^{REV}	Total revenue of the microgrids (\$)
C^{WC}	Wind curtailment cost (\$)
$E_{b,t}^{TESS}$	Energy stored in TESS b at time interval t (kWh)
i	index of buses
int_i	The interruption cost of the load at bus i (\$/kWh)
k	Index for reconfiguration topologies
l	Index for WGTs
$om^{WGT,TESS}$	O&M cost of WGT and TESS (\$/kWh)
p, q	Index for stations of TESS
$P_{i,t}^c$	Active load demand of bus i at time t
$P_{b,p,t}^{ch}, P_{b,p,t}^{dis}$	TESS b charge/discharge in the station p at time interval t
P_{max}^{ch}	The maximum charge power of TESS (kW)
P_{max}^{dis}	The maximum discharge power of TESS (kW)
P_i^{SOP}, Q_i^{SOP}	Active and reactive power of the SOP entering bus i (kW)
P_l^{WGT}, Q_l^{WGT}	Actual active and reactive dispatched generation of WGT l at time interval t (kW)
$P_{max,l,t}^{WGT}$	The maximum dispatched wind generation of WGT l at time t (kW)
$P_{(i,j),t}, P_{(i,j),t}$	Active and reactive power flowing from bus i to bus j
$Q_{i,t}^c$	Reactive load demand of bus i at time t
R^{REV}	Total revenues of the microgrids
S_i^{SOP}	Rating power of the SOP connecting bus i
$SOC_{b,t}$	SOC of TESS b at time interval t (%)
t	Index for hours
$transport_{cost}$	Transport cost of TESS (\$)
V_i	Voltage of bus i

1. Introduction

The safe operation of a future power system running largely on renewable sources while maintaining reliable power supply to customers has become a major research topic and attracted substantive attentions in the last decade. The increasing frequency of natural disasters with high-impact but low-probability (HILP) such as typhoons, floods, wild fires, and heavy snows due to climate change imposes further challenges on the operation and control of future power systems [1, 2]. Most studies agree that the existing infrastructure of power systems has limited their resilience to severe and extreme weather conditions [3, 4]. HILP events may cause line interruption, generator trip, load disconnection and other faults, often leading to disconnection of a number of customers from the power grid, even the disconnection of a whole local network from the main grid [5]. Besides, as the configuration of the modern power systems becomes more complex, the difficulty of power system restoration after failures becomes severer. Therefore, in order to cope with the occurrence of more HILP events, it becomes vital to enhance the power system resilience and reduce the economic losses during the post-disaster restoration process. To increase the resilience of the power system, some studies suggest that the infrastructure of the power system can be reinforced to cope with the damage of natural disasters [6, 7, 8]. However, with the expansion of the power grids to meet ever increasing electricity demand, the infrastructure requiring pre-disaster reinforcement also becomes more numerous and harder to identify, and the reinforcement often involves significant amount of time and costs. Therefore, it is imminent to develop efficient post-disaster restoration schemes based on the existing power system infrastructure.

Studies have shown that, following a disaster, establishing microgrids in isolated areas due to failures by leveraging distributed energy resources or energy storage systems is an effective strategy for post-disaster restoration [9, 10]. Microgrid is referred to a local power generation and distribution system composed of distributed generations, energy storage devices, load and other components of the power system [11, 12]. Akhtar *et al.* [13] proposed a resilience index for a power system consisting of multiple microgrids. The power system is divided into several microgrids, and each microgrid is evaluated using the resilience index and controlled separately to reduce the impact of the disaster. [14] proposed a post-disaster restoration scheme to restore critical loads suffering from power shortage by forming microgrids energized by distribution generations. In [15], a novel post-disaster restoration scheme was proposed, which involves continuous reconfiguration of the distribution system topology based on the maintenance procedure of the repair crew. A hybrid quantum-classical approach was developed to solve the dispatching problem which can effectively accelerate the post-disaster restoration process. Huang *et al.* [16] proposed a distribution network microgrid formation method based on the deep

reinforcement learning to improve the resilience of power systems in the face of extreme events. Arian *et al.* [17] proposed a three-stage resilient operational scheme for distribution systems in the face of natural disasters. This scheme considers the optimal allocation of energy storage systems and addresses the optimal power flow issue during the restoration process. [18] shows that microgrid-based restoration scheme has the potential to assist distribution networks to efficiently recover from large-scale outages. However, during post-disaster restoration, most studies only focus on restoring the loads on critical nodes. Due to the varying end-use customers of the loads, widespread interruption of certain types of normal loads, such as industrial loads, can still lead to significant economic losses. Therefore, alongside prioritizing the restoration of critical loads, it is also essential to consider the restoration of normal loads with different end-use customers comprehensively, thereby minimizing the cost of load interruptions to the greatest extent. To address this, this paper investigates a comprehensive post-disaster restoration testing scheme, which consider various load types and priorities. In this proposed post-disaster restoration scheme, wind turbine generators (WTG) serve as the main sources of energy during the restoration process, soft open points (SOPs) are used to assist topology transformation and TESSs are utilized for the strategic allocation of energy resources.

During the post-disaster recovery process, renewable distributed generators play a vital role as a significant energy source, offering greater flexibility for the restoration of the distribution network. Wind power is a major alternative to conventional energy and one of the fastest growing renewable energy sources [19]. Wind energy is playing an important role in the power system in many countries and regions, and the mass utilization of renewable energy such as wind energy can play a positive role in enhancing the resilience of the distribution network [20, 21]. In [22], a two-stage stochastic optimization model considering network reconfiguration and wind power allocation was proposed to improve the resilience of the distribution system in the face of disasters. [23] shows that the resilience of the distribution system can be significantly improved in the face of hurricane events by strategically rescheduling the distributed generator units and curtailing the load demands. Additionally, flexible voltage controllers are introduced to address voltage imbalances caused by the uncertainty of wind energy. In [24], a self-healing strategy for distribution system considering wind energy was proposed to reduce the economic costs during the post-disaster period. Krishnamurthy *et al.* [25] shows that using wind turbines generators (WTGs) and diesel generators to supply power collaboratively to the microgrid in islanded mode can improve the resilience of the microgrid. For the distribution system with large-scale wind power integration, Chi *et al.* [26] proposed a set of voltage resilience indicators to dynamically evaluate the voltage performance and the resilience of the distribution system. In [27], the

impact of wind energy and load uncertainties on the resilience of the distribution system is investigated, and it is verified that the post-disaster restoration efficiency can be greatly enhanced by employing dynamic microgrid formation and demand response management. However, considering the non-dispatchable nature of wind energy, most of these studies only focused on utilizing stationary energy storage systems to assist in enhancing the resilience of the distribution system. In fact, due to the high uncertainty of natural disasters, the topology of the distribution system also needs to be reconfigured based on fault conditions following a disaster. Stationary energy storage systems may face challenges in seamlessly adapting to the evolving topology of the distribution system, thereby limiting their effectiveness.

Our society is often supported by both the power and transport networks, and these networks overlap at different geographical locations and nodes, hence the transportable energy storage system (TESS) moving along the transport network have been advocated to improve the resilience of the power system [28]. TESS can dispatch energy between various microgrids, thus improving the resilience of the entire power system and reducing the loss of post-disaster recovery due to its mobility and flexibility [29]. In [30], the arrangement of transportable energy storage systems considers the distribution of energy resources in the distribution system as well as the scheduling of the repair team, thus the load curtailment caused by disasters can be effectively reduced. Yao *et al.* [31] designed a spatial-temporal model for TESS operation and proposed a joint restoration scheme with TESS and network reconfiguration in microgrids to reduce the economic costs of distribution systems during the post-disaster recovery. In [32], TESS is integrated into the security constraint unit commitment problem model to provide a secure and resilient scheme for the coastal distribution grids. Kim *et al.* [33] proposed a two-stage stochastic optimization model and used TESS to form dynamic microgrids to reduce disaster damage to distribution networks. In summary, transportable energy storage systems can assist more reasonable distribution of energy during the post-disaster recovery of the distribution network, thereby enhancing the efficiency of the restoration process. Furthermore, considering the randomness of fault occurrences, it is essential to form microgrids for post-disaster recovery by adjusting the topology of the network through tie switches or soft open points (SOPs) [34, 35]. SOPs are power electronic devices that can replace traditional tie switches, and they can help achieve rapid supply restoration and fault isolation after power outages in the face of extreme conditions [36]. During the microgrid formation and topology change phase, SOPs can continuously adjust and control the power flow and voltage, thereby improving the efficiency of the power grid during the post-disaster recovery [37]. Hence, the combination of SOP and transportable energy storage systems has the potential to offer greater flexibility and higher efficiency for the post-disaster recovery of the distribution

networks.

In this paper, a restoration scheme based on wind turbine generators, transportable energy storage systems and network reconfiguration assisted with SOPs is proposed. Considering the randomness of disaster occurrences, the proposed post-disaster recovery scheme first utilizes SOPs to perform topology reconfiguration considering the fault conditions. By forming post-disaster microgrids, the fault areas are isolated, becoming external to the formed microgrids, thereby ensuring that all load buses can be effectively restored, immune to the impacts propagated from the fault areas. It should be noted that if a HILP event occurs, resulting in the entire distribution system being disconnected from the main grid, the microgrids formed for post-disaster recovery will rely primarily on wind energy as their main power source in the proposed restoration scheme. Given the inherent uncertainty of wind energy, it is essential to equip the wind power generators with energy storage systems to improve their dispatchability and assist with frequency and voltage control for the microgrids. If a microgrid has more than one generator, the voltage and frequency control often adopt either the master-slave mode or power sharing mode, depending on the size of the generators and the load conditions. The proposed post-disaster recovery scheme primarily evaluates the post-disaster recovery cost during load interruptions as its main assessment criterion. It comprehensively considers the differences in interruption costs for critical and normal loads, as well as different load types under fault scenarios. Furthermore, taking into account the uncertainty of wind energy, this paper has selected multiple wind power output scenarios to further validate the effectiveness of the proposed post-disaster recovery scheme. The comparison of this study with existing works is summarized in Table 1. The main contributions are summarized as follows:

1. A novel post-disaster restoration scheme of distribution networks considering TESS, SOP and wind turbine generators is established, and an economic model is formulated to evaluate the effectiveness of the proposed scheme.
2. Taking into account the stochastic nature of fault occurrences, this paper has designed a diverse set of fault scenarios, encompassing factors such as the timing of fault occurrences and the randomness of wind power output.
3. The proposed post-disaster restoration scheme not only focuses on the restoration of critical loads but also takes into account the comprehensive pickup of specific types of normal loads with relatively high interruption costs, thereby further enhancing the economic viability.

The rest of this paper is organized as follows: Section 2 introduces SOP and TESS. Section 3 presents the proposed model formulation. Extensive numerical studies and

result analyses are presented in Section 4. Discussion and conclusion are given in Section 5 and Section 6.

2. Introduction to SOP and TESS

This section presents the preliminaries of the models for TESS and SOP. SOP can be used to efficiently adjust the topologies of the power grid, thus helping the grid to form microgrids to recover from HILP events [38]. While the TESS's mobility offers more flexibility in energy dispatch within the power grids, thus increases the resilience of distribution networks in face of HILP events.

2.1. Modelling of SOP

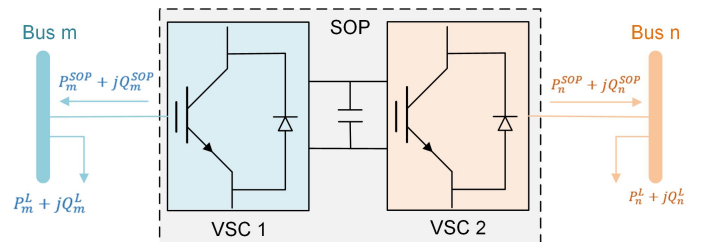


Figure 1: Power injection model of SOP

SOP can help the distribution network to achieve flexible power control, and a back-to-back voltage source converter (VSC) based SOP is shown in Fig 1. There are two common SOP control modes, namely power flow mode and power supply restoration mode. In the power flow control mode, SOP can bidirectionally provide both active and reactive power. In this mode, VSC1 works on the $P-Q$ control scheme whilst VSC2 operates on the $V_{dc} - Q$ control scheme. If a fault occurs on the VSC2 side, loads at the feeder are lost and the frequency and voltage of VSC2 are decoupled from the grid. In this case, VSC2 would be switched to the $V_{ac} - \theta$ control scheme. Simulation results show that SOP can successfully switch among different modes within seconds. The problems of current offset and inrush are solved in the process of mode transition, which reduces unexpected protection operations [39].

The active power constraint of SOP is given as follows:

$$P_m^{SOP} + P_n^{SOP} + P_{loss}^{SOP} = 0 \quad (1)$$

where P_m^{SOP} and P_n^{SOP} denote the active power of SOP entering feeder ends at bus m and n , respectively. P_{loss}^{SOP} is the internal power loss of the SOP. For a high efficiency SOP, P_{loss}^{SOP} is very small and can be neglectable. It becomes:

$$P_m^{SOP} + P_n^{SOP} = 0 \quad (2)$$

The reactive power outputs of SOP are independent, which implies both power compensation and absorption are available. The operational limits of power entering the feeders are constrained by the capacities of the two symmetrical VSCs, it follows

$$\|P_m^{SOP} + jQ_m^{SOP}\| \leq S_m^{SOP} \quad (3)$$

Table 1: Comparison between this study and existing works.

Ref	Year	Load Priority	Load Type	TESS	SOP	RGs	Topo Reconfiguration	Test System Scale
[13]	2019	×	✓	×	×	✓	×	33-bus
[15]	2023	×	×	×	×	✓	✓	9-bus & 23-bus
[16]	2022	✓	×	×	×	✓	✓	37-bus & 123-bus
[17]	2023	✓	×	×	×	×	✓	33-bus
[18]	2021	✓	×	×	×	✓	✓	37-bus & 123-bus
[23]	2022	×	×	×	×	✓	×	33-bus & 123-bus
[27]	2020	×	×	×	×	✓	✓	33-bus & 492-bus
[30]	2023	×	×	✓	×	✓	✓	33-bus
[32]	2020	×	×	✓	×	✓	×	69-bus
[38]	2020	×	×	×	✓	✓	✓	33-bus
This Study	-	✓	✓	✓	✓	✓	✓	33-bus & 69-bus

$$\|P_n^{sop} + jQ_n^{sop}\| \leq S_n^{sop} \quad (4)$$

where S_m^{SOP} and S_n^{SOP} are the rating power of VSC1 and VSC2, respectively.

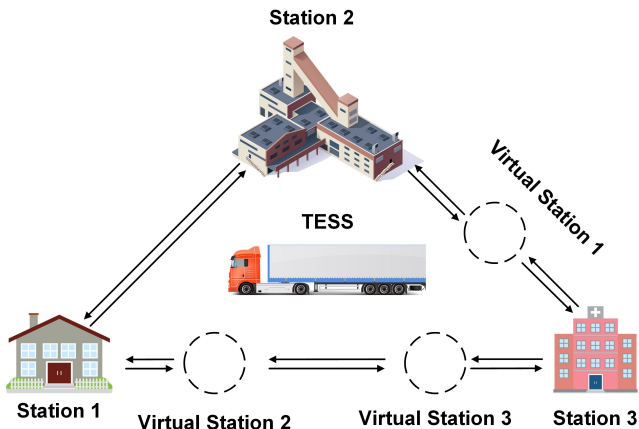


Figure 2: The schematic road grid of a TESS.

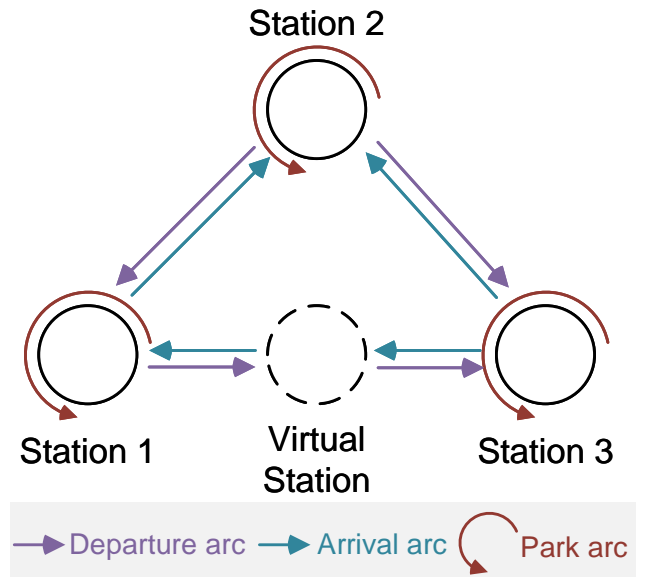


Figure 3: Transition diagram for TESS.

2.2. Modelling of TESS

A TESS refers to a compact and mobile system that consists of battery cells and a bidirectional power converter [40]. Unlike the stationary energy storage system, TESS is installed in a container which is mounted either on a truck to move along a road network or in a railway carriage along a railway network to achieve mobility. The charging/discharging schedule of the TESS is therefore combined with the routing problem.

Time-space network (TSN) is an approach that is widely used for modeling the routing schedule of vehicles and railways [31, 41]. It is suitable to demonstrate the variations of spatial components as well as temporal intervals. Considering the variable distances between different TESS stations, virtual stations are introduced to assist defining the TSN model for the TESS. The introduction of the virtual station essentially aims to align the state transition

of TESS with the decision horizon of the proposed post-disaster recovery model. Specifically, if TESS cannot reach the target station within a decision horizon, it is assumed that TESS will reach a virtual station after traversing the decision horizon, thereby making the TSN model solvable. It is important to note that TESS cannot park, charge, or discharge at these virtual stations. The travelling time interval between any two stations is a decision horizon, which is defined as 1 hour in this study. Fig 2 illustrates a simple road grid of a TESS, which has three real stations and three virtual stations. As shown in Fig 2, TESS can shuttle between different types of loads and provide services to the required loads. Fig 3 illustrates the transition diagram of TESS, indicating that TESS can only charge or discharge when it is located within the Park arc. The introduction of virtual stations is to ensure that the state of TESS is defined at any decision horizon in the proposed

model. Since the virtual stations do not have physical presence, TESS will not perform charging or discharging operations there.

The TSN-based transportation model of TESS is formulated as follows:

$$\sum_{(p,q) \in \mathbb{Q}} \gamma_{b,(p,q),t} = 1, \forall b \in \mathbb{B}, t \in \mathbb{T} \quad (5)$$

$$\sum_{p \in \mathbb{Y}^+} \delta_{b,p,0} = 1, \forall b \in \mathbb{B} \quad (6)$$

$$\sum_{(p,q) \in \mathbb{Q}_p^+} \gamma_{b,(p,q),t+1} = \sum_{(p,q) \in \mathbb{Q}_p^-} \gamma_{b,(p,q),t}, \forall p \in \mathbb{Y}, t \in \mathbb{T} \quad (7)$$

$$\sum_{(p,q) \in \mathbb{Q}_p^+} \gamma_{b,(p,q),1} = \delta_{b,p,0}, \forall p \in \mathbb{Y}^+ \quad (8)$$

$$\gamma_{b,(p,q),t} + \gamma_{b,(q,p),t+1} \leq 1, \forall b \in \mathbb{B}, (p,q) \in \mathbb{Q}, p \neq q \quad (9)$$

Constraint (5) defines the state of TESS b at time interval t by binary variable $\gamma_{b,(p,q),t}$, \mathbb{B} is the set of TESSs, \mathbb{T} is the set of time spans where $\mathbb{T} = \{0, 1, \dots, t\}$. In any time span, TESS b either transits from station p to station q or stays still. (p, q) represents the transit arc/park arc. If p is the same as q , it is a park arc. Otherwise, it is a transit arc. \mathbb{Q} is set of arcs. Constraint (6) defines the initial position of TESS b at time interval 0. If TESS b locates at station p , the binary variable $\delta_{b,p,0}$ is 1. Otherwise, it is 0. \mathbb{Y}^+ is set of real stations along a transport network. Constraint (7) states that if the TESS b is at the station p at the end of time interval t , it must be in the arc that starts from the station p at the next time interval $t+1$. \mathbb{Q}^+ is the set of arcs starting from the station p and \mathbb{Q}^- is the set of arcs ending at the station p . \mathbb{Y} is the set of stations including both real stations and virtual stations. The initial transportation state of TESS b is declared in constraint (8), which is related to its initial position. Constraint (9) enforces TESS can not return immediately to the station where it travels from at the previous time interval because there is no point in doing so.

When considering spatial displacement, only on park arcs can TESS charge from or discharge to the grid. The related constraints can be shown as follows:

$$0 \leq \eta_b^{ch} P_{b,p,t}^{ch} \leq \gamma_{b,(p,p),t} P_{max}^{ch}, \forall b \in \mathbb{B}, p \in \mathbb{Y}^+, t \in \mathbb{T} \quad (10)$$

$$0 \leq \frac{P_{b,p,t}^{dis}}{\eta_b^{dis}} \leq \gamma_{b,(p,p),t} P_{max}^{dis}, \forall b \in \mathbb{B}, p \in \mathbb{Y}^+, t \in \mathbb{T} \quad (11)$$

$$0 \leq \eta_b^{ch} \sum_{p \in \mathbb{Y}^+} P_{b,p,t}^{ch} \leq \varphi_{b,t}^{ch} P_{max}^{ch}, \forall b \in \mathbb{B}, t \in \mathbb{T} \quad (12)$$

$$0 \leq \frac{\sum_{p \in \mathbb{Y}^+} P_{b,p,t}^{dis}}{\eta_b^{dis}} \leq \varphi_{b,t}^{dis} P_{max}^{dis}, \forall b \in \mathbb{B}, t \in \mathbb{T} \quad (13)$$

where $P_{b,p,t}^{ch}$ and $P_{b,p,t}^{dis}$ are charging and discharging power from/to grid of TESS b in the station p at time interval t , respectively. η_b^{dis} is charging efficiency of TESS b and η_b^{dis}

is corresponding discharge efficiency. $\varphi_{b,t}^{ch}$ and $\varphi_{b,t}^{dis}$ are binary variables that represent the charging/discharging states of TESS b at time interval t . Based on the TSN model, $\sum_{p \in \mathbb{Y}^+} \gamma_{b,(p,p),t}$ is 1 when there exists park arc at time interval t . In this case, there are three possible operation modes of the TESS b : charging, discharging and idle mode. However, when TESS b is on transit arc, the TESS neither charge nor discharge and $\sum_{p \in \mathbb{Y}^+} \gamma_{b,(p,p),t} = 0$. (10) and (11) ensure that TESS can only perform charging and discharging operations when it is in park arc. (12) and (13) respectively specify the charging and discharging limits for TESS within a decision horizon.

The constraints of operation modes of TESS are given below:

$$\varphi_{b,t}^{ch} + \varphi_{b,t}^{dis} \leq \sum_{p \in \mathbb{Y}^+} \gamma_{b,(p,p),t}, \forall b \in \mathbb{B}, t \in \mathbb{T} \quad (14)$$

$$E_{b,t+1}^{TESS} = E_{b,t}^{TESS} + \eta_b^{ch} \sum_{p \in \mathbb{Y}^+} P_{b,p,t}^{ch} \Delta t - \frac{\sum_{p \in \mathbb{Y}^+} P_{b,p,t}^{dis}}{\eta_b^{dis}} \Delta t, \quad \forall b \in \mathbb{B}, t \in \mathbb{T} \setminus \{0\} \quad (15)$$

$$SOC_{b,t} = \frac{E_{b,t}^{TESS}}{C_b^{TESS}}, \forall b \in \mathbb{B}, t \in \mathbb{T} \quad (16)$$

$$SOC_{min} \leq SOC_{b,t} \leq SOC_{max}, \forall b \in \mathbb{B}, t \in \mathbb{T} \quad (17)$$

Constraint (14) ensures that within a decision horizon, TESS cannot simultaneously perform charging and discharging operations. Equations (15) and (16) dynamically calculate the energy stored in TESS and the SOC for TESS. Constraint (17) ensures that the SOC of TESS can not exceed its predefined upper or lower limits at any given time.

3. Problem Formulation

This section presents an economic cost model that considers the post-disaster restoration scheme based on the TESS, SOP, and wind energy. The objective function and the related constraints are introduced as follows.

3.1. Objective function

In the restoration period, the objective function Ob aims to minimize the total costs which consist of the load interruption cost C^{INT} , operation and maintenance (O&M) cost of wind turbine generators and TESS (C^{OM}), wind curtailment cost (C^{WC}), transportation cost of TESS (C^{POS}) and maximize the total revenue of the microgrids (C^{REV}). The objective function can be shown as follows:

$$\begin{aligned} Ob &= \min F(\mathbf{P}_k) \\ &= \min(C^{INT} + C^{OM} + C^{WC} + C^{POS} - C^{REV}) \end{aligned} \quad (18)$$

where

$$C^{INT} = \sum_t \left[\sum_i C^{int_i} (P_{i,t}^c - P_{i,t}^{rc}) \Delta t \right] \quad (19)$$

$$C^{OM} = \sum_t \left(\sum_j om_j^{WTG} + \sum_b om_b^{TESS} \right) \quad (20)$$

$$C^{WC} = \rho^{WC} \sum_t \sum_j (P_{j,t}^{WTG} - P_{real,j,t}^{WTG}) \Delta t \quad (21)$$

$$C^{POS} = \sum_t \sum_b pos_b \sum_{(p,q) \in \mathbb{Q}, p \neq q} \gamma_{b,(p,q),t} \quad (22)$$

$$C^{REV} = \rho^c \sum_t \sum_i P_{i,t}^{rc} \Delta t \quad (23)$$

\mathbf{P}_k in Equation (18) represents the selected topology based on SOP of the distribution network in the post-disaster restoration period. In Equation (19), C^{int_i} is the interruption cost for the load at bus i . $(P_{i,t}^c - P_{i,t}^{rc})$ computes the difference between the normal demand of load i at time t and the demand that can be covered during the post-disaster recovery period. The interruption cost of critical loads is much higher than normal loads in order to guarantee the priority of restoration order. C^{OM} in Equation (20) represents the operation and maintenance costs of all WTGs and TESSs during the operating horizon. om^{WTG} and om^{TESS} are O&M costs for WTGs and TESS (\$/kWh) in the time interval t . C^{WC} is wind curtailment cost. $P_{j,t}^{WTG}$ and $P_{real,j,t}^{WTG}$ are maximal potential generation power and actual dispatched generation power of WTG j at time interval t , respectively. ρ^{WC} is the price of wind curtailment (\$/kWh). C^{POS} is the transportation cost of TESS. If TESS is on the transit arc that $(p, q) \in \mathbb{Q}, p \neq q$, then $\gamma_{b,(p,q),t} = 1$. $pos_{b,t}$ is the cost per unit of time (\$/kWh) to transport the TESS b . The final term C^{REV} describes the total revenues achieved by selling the electricity to the customers at price ρ^c (\$/kWh) during the restoration process.

3.2. Constraints

Due to the requirements of the safe operation of the distribution network, the relevant constraints of the distribution network should always be met in the process of post-disaster recovery. Otherwise, the distribution network may collapse, which would lead to the failure of the whole restoration process or even more serious consequences.

3.2.1. Power flow constraints

When an extreme weather event occurs, the distribution network may suffer several line faults. After reconfiguration, the power flow model for each new microgrid a to restore loads is given as follows:

$$\begin{aligned} \sum_{(i,j) \in \mathbb{E}_a} P_{(i,j),t} &= \sum_{(h,i) \in \mathbb{E}_a} P_{(h,i),t} - P_{i+1,t}^{rc} + P_{i+1,t}^{WTG} \\ &\quad - \gamma_{(i,i),t} P_{i,t}^{ch} + \gamma_{(i,i),t} P_{i,t}^{dis} \forall i \in \mathbb{N}_a, t \in \mathbb{T} \end{aligned} \quad (24)$$

$$\sum_{(i,j) \in \mathbb{E}} Q_{(i,j),t} = \sum_{(h,i) \in \mathbb{E}} Q_{(h,i),t} - Q_{i+1,t}^{rc} + Q_{i+1,t}^{DG} \quad (25)$$

$$0 \leq P_{i,t}^{rc} \leq P_{i,t}^c, \forall i \in \mathbb{N}, t \in \mathbb{T} \quad (26)$$

$$Q_{i,t}^{rc} = P_{i,t}^c \tan[\cos^{-1}(pf_i^c)], \forall i \in \mathbb{N}, t \in \mathbb{T} \quad (27)$$

$$\|P_{(i,j),t} + jQ_{(i,j),t}\| \leq S_{(i,j),t}, \forall (i,j) \in \mathbb{E} \quad (28)$$

$$V_{j,t} = V_{i,t} - \frac{r_{(i,j)} P_{(i,j),t} + x_{(i,j)} Q_{(i,j),t}}{V_0}, \forall (i,j) \in \mathbb{E}, t \in \mathbb{T} \quad (29)$$

$$V_{min} \leq V_{i,t} \leq V_{max}, \forall i \in \mathbb{N}, t \in \mathbb{T} \quad (30)$$

where \mathbb{E}_a and \mathbb{N}_a are branch and bus sets of microgrid a . $\gamma_{(i,i),t}$ represents the status of TESS at bus i , with a value of 0 whenever TESS does not park at that bus. $P_{(i,j),t}$ and $Q_{(i,j),t}$ are active and reactive power flows from bus i to bus j respectively. $r_{(i,j)}$ and $x_{(i,j)}$ are resistance and reactance between bus i and bus j . $P_{i,t}^{WTG}$ and $Q_{i,t}^{WTG}$ are corresponding active/reactive power generations of WTG at bus i . $V_{i,t}$ is the voltage at bus i and V_0 is the reference voltage. Constraints (24) and (25) ensure the active power and reactive power balance on the line from bus i to bus j . The Constraint (26) enforces the upper and lower boundary on restored active load $P_{i,t}^{rc}$. Equation (27) calculates the reactive power with the load power factor pf_i^c of each bus i . Constraint (28) ensures that the composite value of active power and reactive power from bus i to bus j does not exceed the apparent power at the corresponding time. The voltage drop from bus i to bus j is calculated using Equation (29). Constraint (30) is the operation limits of voltage magnitude.

3.2.2. Network topology constraints

Since the restoration scheme proposed in this paper is based on microgrids, after a fault occurs, the original distribution network will be divided into several microgrids with the assistance of SOPs for post-disaster recovery. During the process of forming microgrids, network topology constraints need to be taken into consideration. In summary, the network topology constraints mainly include network splitting constraints, sub-network connectivity constraints, and sub-network radial constraints.

1) *Network splitting constraints*: Firstly, when forming microgrids during the post-disaster restoration process, each bus or line should only belong to one microgrid. This is because different microgrids rely on their own distributed generators as the primary energy source, the frequencies, voltages, and phases are usually different among these microgrids. The interconnection of these microgrids could potentially impact the efficiency of restoration. These constraints can be expressed using the following equations:

$$\sum_{m=1}^{NM} sob_{b,t}^m = 1 \quad (31)$$

$$\sum_{m=1}^{NM} sol_{l,t}^m = 1 \quad (32)$$

where NM represents the number of microgrids formed in the post-disaster restoration process. $sob_{b,t}^m$ and $sol_{l,t}^m$ represent the energized status of bus b and line l at t^{th} time interval in the m^{th} microgrid, respectively. It should be noted that both of these two variables are binary variables and can only equal 1 when the bus or line is within its corresponding microgrid.

Furthermore, if line l belongs to microgrid m , both the source bus and the sink bus of this line should belong to this microgrid, which can be expressed as follows:

$$sol_{l,t}^m \leq sob_{l_{source},t}^m \quad (33)$$

$$sol_{l,t}^m \leq sob_{l_{sink},t}^m \quad (34)$$

where $sob_{l_{source},t}^m$ and $sob_{l_{sink},t}^m$ are the source and sink buses of line l .

2) *Sub-network connectivity constraints*: When forming microgrids, there should be corresponding connectivity constraints of the buses and lines within the microgrid.

For buses directly connected to distributed generators, they should always be energized during post-disaster restoration, which can be shown as:

$$sob_{b_{DG},t}^m = 1 \quad (35)$$

For the buses that are not connected to the generators, the constraints of the buses and their related lines can be expressed as:

$$sob_{b,t}^m = sol_{l^b,t}^m \quad (36)$$

$$sol_{l,t}^m = sob_{b,t}^m \quad (37)$$

where $sol_{l^b,t}^m$ is the line with bus b as the source bus, and $sol_{l^b,t}^m$ is the line with bus b as the sink bus.

3) *Sub-network radial constraints*: During the post-disaster microgrid formation process, it is essential to maintain radial network topology centered around the grid-forming generators. To establish a radial network topology, the difference between the number of buses and the number of lines in the microgrid must be 1, and all sub-tour must be eliminated. The radial network topology constraints can be shown as:

$$\sum_{l=1}^{NL} sol_{l,t}^m = \sum_{b=1}^{NB} sob_{b,t}^m - 1 \quad (38)$$

$$sol_{(a,b),t}^m + sol_{(b,a),t}^m = 1 \quad (39)$$

where NL and NB represent the number of lines and buses in the microgrid. $sol_{(a,b),t}^m$ represents the line with bus a as the source bus and bus b as the sink bus. Constraint (39) ensures that within a decision horizon, the power flow in the microgrid is unidirectional.

3.2.3. Other operation constraints

The charging/discharging power to the grid at bus i is dependant on the status of TESS. If the station p is located

at bus i , it is represented by the symbol $p \downarrow i$. When TESS b parks at station p , then the following equations hold:

$$P_{i,t}^{ch} = \sum_b P_{b,p,t}^{ch}, \forall i \in \mathbb{N}, t \in \mathbb{T}, p \downarrow i \quad (40)$$

$$P_{i,t}^{dis} = \sum_b P_{b,p,t}^{dis}, \forall i \in \mathbb{N}, t \in \mathbb{T}, p \downarrow i \quad (41)$$

where $P_{b,p,t}^{ch}$ and $P_{i,t}^{dis}$ represent the power of TESS b for charging and discharging at station p , respectively. TESS is only permitted to charge or discharge when parked at station p . Otherwise, $P_{b,p,t}^{ch}$ and $P_{i,t}^{dis}$ must both be zero.

The maximal active power generated by WTG, denoted as $P_{max,i,t}^{DG}$ depends on the installed capacity of the WTG. The power generation of WTG in any time interval cannot exceed the installed capacity, which can be shown as follows:

$$0 \leq P_{i,t}^{WTG} \leq P_{max,i,t}^{WTG} \quad (42)$$

Aided with the power electronic device, i.e. inverter interface, WTG is capable of adjusting its reactive power to satisfy the power factor pf_i^{WTG} required by the system operator. The operation constraints of the adjustable inverter-interfaced WTG are mathematically formulated as:

$$-P_{i,t}^{WTG} \cdot \tan \left[\cos^{-1}(pf_i^{WTG}) \right] \leq Q_{i,t}^{WTG}$$

$$Q_{i,t}^{WTG} \leq P_{i,t}^{WTG} \cdot \tan \left[\cos^{-1}(pf_i^{WTG}) \right], \forall i \in \mathbb{N}, t \in \mathbb{T} \quad (43)$$

where pf_i^{WTG} enforces the power factor of each generator.

4. Numerical Results

In this section, a wide range of fault scenarios are investigated to verify the effectiveness of the proposed restoration scheme. All the simulation results in this study are implemented with CPLEX 12.8.0 using computer with an Inter(R) Core(TM) i5-6400 CPU at 2.7 GHz.

4.1. Introduction to the test system and fault scenarios

In this study, the resilient operation is implemented on a modified IEEE 33-bus system at first, as shown in Fig 4. The original configuration has five tie switches, two WTGs, 33 load buses, 32 transmission lines and one TESS. In the proposed modified IEEE 33-bus system, all loads are categorized into critical loads and normal loads based on their restoration priority. Critical loads, such as servers, security systems, and life support equipment for hospitals often incur the highest interruption cost. Additionally, all loads can be further classified into industrial, commercial, and residential loads based on the type of end-users, each having distinct interruption costs for normal loads [42]. Fig 7 illustrates the interruption costs for various load priorities and types. As shown in Fig 7, all critical loads

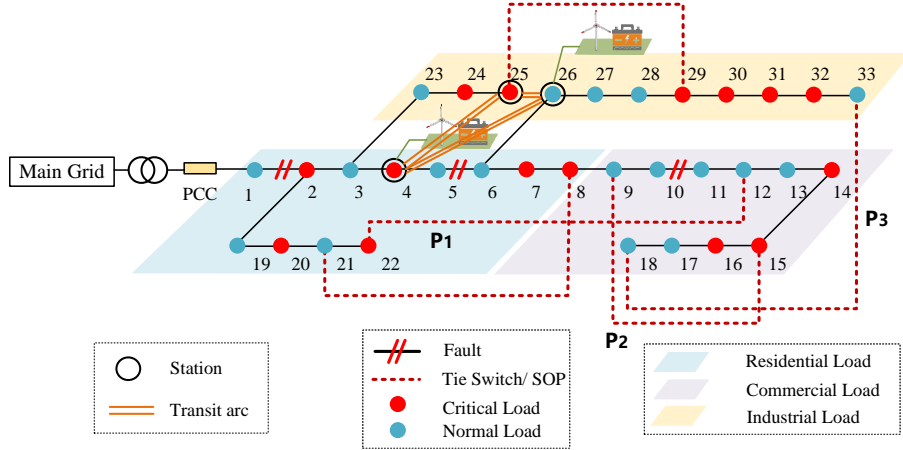


Figure 4: The schematic test system.

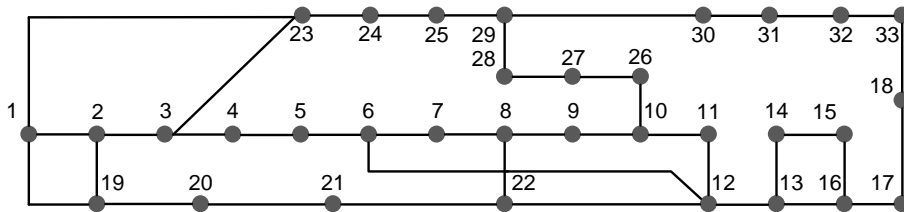


Figure 5: Transportation network mapped from the modified 33-bus test system.

have the highest interruption costs, ensuring their priority for restoration during post-disaster recovery. As for the three types of normal loads, the interruption costs are arranged in descending order from industrial, commercial to residential. Tie switches play a crucial role in system reconfiguration during line faults. However, tie switches are passive devices and do not offer power flow control capability. Thus, in this study, to improve the effectiveness of the restoration scheme, the tie switches are replaced by SOPs. Further, the scheduling of TESS needs to consider the transportation network layout. Therefore, a simplified transportation network is designed based on the distribution network [43]. Fig 5 illustrates the layout of the proposed transportation network, where the nodes of this network correspond to the buses of the distribution system, and each edge represents a bidirectional route. For the convenience of analysis, this study assumes the uniform distance between any two buses in the transportation network, and TESS can traverse maximally 5 buses within one decision horizon.

Fig 4 shows the failure scenario considered in this paper, i.e. the line faults occur on lines (1, 2), (5, 6), (10, 11). The test system loses connection from the main grid and loses the loads from Bus 11 to Bus 18. Two islanded microgrids powered by WTGs are formed with network reconfiguration. Besides, this study further considers fault scenarios that occur in three periods of time such that the fault scenarios considered are more comprehensive, which is shown in Fig 6. The three scenarios are defined as follows:

- Scenario 1: Power surplus occurs during the restora-

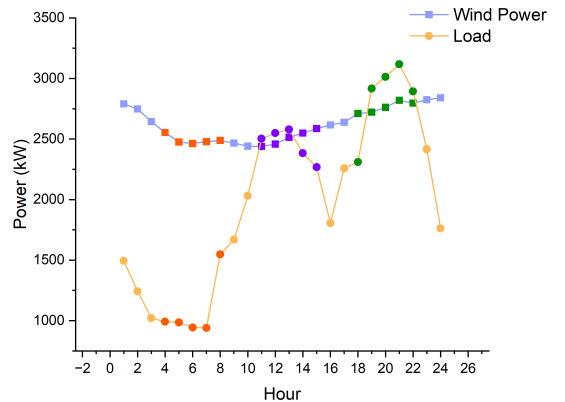


Figure 6: Fault scenarios under different time of period.

tion period (4 : 00 – 8 : 00).

- Scenario 2: Both power surplus and shortage occur during the restoration period (11 : 00 – 15 : 00).
- Scenario 3: Power shortage occurs during the restoration period (18 : 00 – 22 : 00).

In addition, the parameter settings for the test system can be shown in Table 2.

4.2. Topology reconfiguration based on SOP

According to the failure scenarios proposed in this study, there are three possible reconfiguration topologies to pick up the loads from Bus 11 to Bus 18, which are shown in

Table 2: Parameter setting for the test system.

Item	Parameters
WGT-I Capacity in Bus 4 (MW)	850
WGT-II Capacity in Bus 26 (MW)	2000
TESS Charge Efficiency (%)	99
TESS Discharge Efficiency (%)	92
Initial SOC of TESS	0.5
SOC_{min} of TESS	0
SOC_{max} of TESS	0.9
Critical Load interruption Cost (\$/kWh)	10
Normal Load interruption Cost (\$/kWh)	2

Table 3: Simulation results of different topologies with tie switches under different scenarios.

Scenario	Scenario 1		Scenario 2		Scenario 3	
	Tie Switch	SOP	Tie Switch	SOP	Tie Switch	SOP
Total Cost (\$)	18420.6	8324.69 (54.8% ↓)	21928.46	11810.64 (46.14% ↓)	49307.94	23720.33 (51.89% ↓)
Critical Load Restoration (%)	45.43	72.12 (26.69% ↑)	59.1	80.19 (21.09% ↑)	45.04	71.04 (26% ↑)
Normal Load Restoration (%)	36.80	93.08 (56.28% ↑)	53.32	85.01 (31.69% ↑)	60.16	88.83 (28.67% ↑)
Total Load Restoration (%)	42.53	79.16 (36.63% ↑)	57.1	81.86 (24.76% ↑)	49.16	75.89 (26.73% ↑)

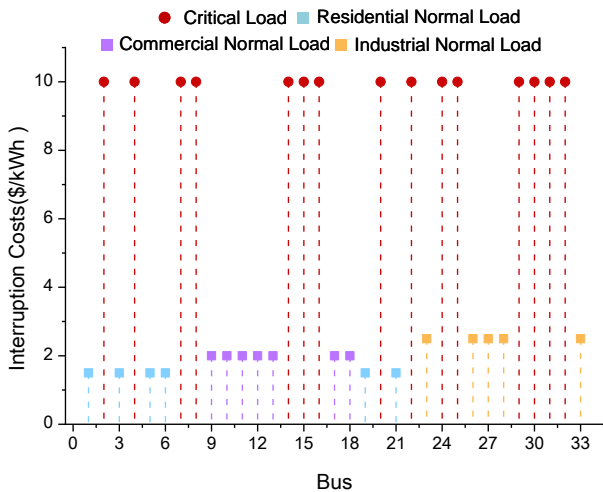


Figure 7: Interruption costs for various load priorities and types.

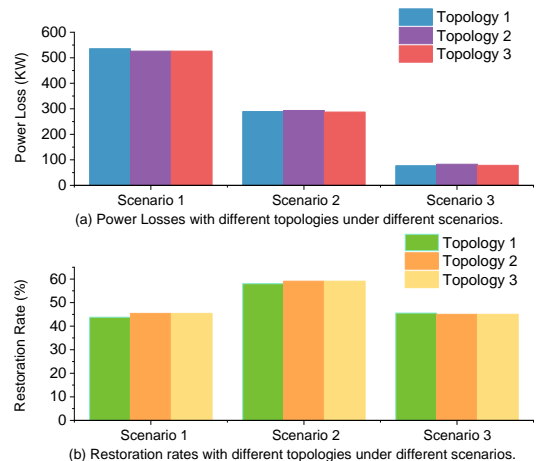


Figure 8: Simulation results of different topologies with tie switches under different scenarios.

Fig 4. These three topologies can be represented by \mathbf{P}_1 , \mathbf{P}_2 , and \mathbf{P}_3 respectively.

Fig 8 compares the power losses and the restoration rate under the three topologies. As shown in Fig 8, \mathbf{P}_3 is relatively more effective for the three scenarios considering in this study. Therefore, in the following experimental analysis, the topology of \mathbf{P}_3 is chosen to study the proposed fault scenarios, as shown in Fig 9.

As mentioned above, SOP is used to replace the tie switches. When SOP is used, the loads restoration and related economic costs under the three scenarios with topology \mathbf{P}_3 are listed in Table 3. As shown in Table 3, the load restoration rates with SOP in the three scenarios have

been greatly improved, with the maximum improvement of 36.63%. Besides, the total economic costs required during the restoration period have been significantly reduced, and the maximum reduction is 54.8%.

Fig 10 shows a comparison between SOP and tie switch during the post-disaster recovery. When SOP is used to connect Bus 18 and Bus 33, the transmission power between the two buses remains above $400kW$, which is always higher than that with tie switch. This is because SOP is a controlled energy transmission equipment that can transmit as much energy as allowed to the required buses in the face of failure scenarios. As a result, the loads from Bus 11 to Bus 18 can be restored more efficiently. The

Table 4: Simulation results of different station selection options under different scenarios.

Scenario	Scenario 1		Scenario 2		Scenario 3	
Initial Position	Option 1	Option 2	Option 1	Option 2	Option 1	Option 2
Total Cost (\$)	4402.45	3355.17	8442.14	7572.59	22744.11	21667.39
Critical Load Restoration (%)	85.48	88.32	85.94	87.89	75.29	77.03
Normal Load Restoration (%)	93.08	95.97	81.37	75.26	84.4	76.67
Total Load Restoration (%)	88.03	90.89	84.36	83.52	77.77	76.93

* **Option 1** corresponds to (Bus 14, Bus 4, Bus 26); **Option 2** corresponds to (Bus 25, Bus 4, Bus 26).

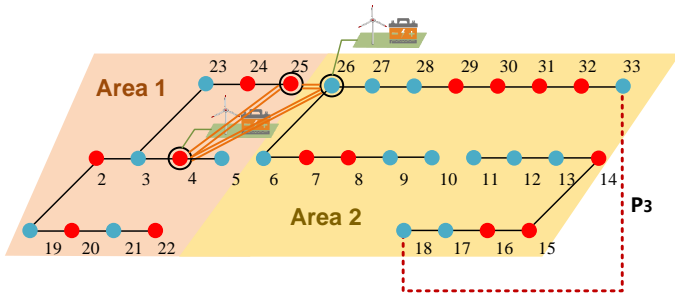


Figure 9: The topology with P_3 .

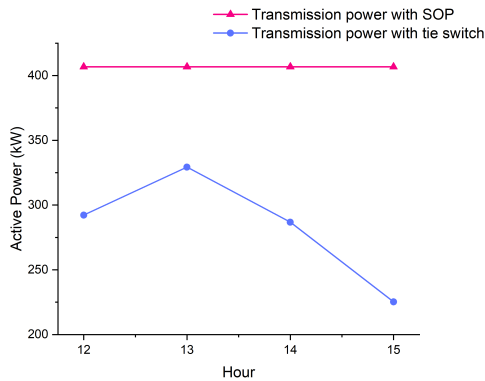


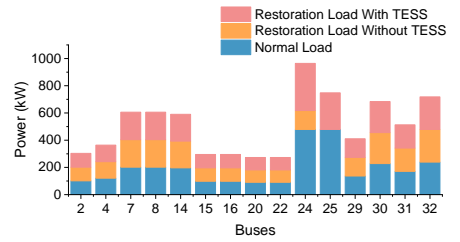
Figure 10: Transmission Power between Bus 18 and 33 in Scenario 2.

results above demonstrate the positive role that SOP can play during the post-disaster restoration period.

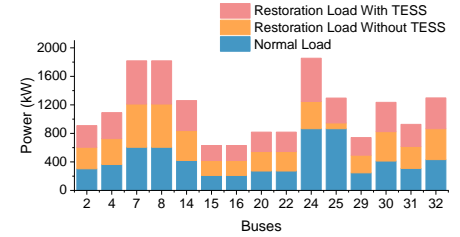
4.3. The effects of TESS in post-disaster restoration

4.3.1. The TESS stations selection

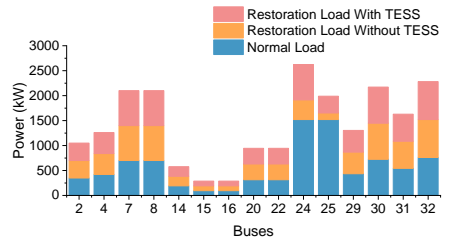
When using TESS to support post-disaster restoration, the stations to host the TESS need to be identified firstly. Considering the uncertainty of HILP events, the fault locations are also unpredictable. To ensure that TESS can perform flexible charging and discharging scheduling after a disaster, buses connected to distributed generators should be prioritized as potential stations for TESS. This is because these buses can provide power for restoration thus offer greater flexibility for scheduling the TESS under various fault conditions. Based on this principle, in the



(a) Critical Load in Scenario 1.



(b) Critical Load in Scenario 2.



(c) Critical Load in Scenario 3.

Figure 11: Critical load analysis under different scenarios.

proposed modified IEEE 33-bus system, Bus 4 and Bus 26, which are connected with wind turbine generators, are selected as the two TESS stations. Further, to improve the restoration efficiency, critical buses located at the end of microgrids with significant demands should also be considered as potential TESS stations. Since these buses are located at the terminus of formed microgrids, energy resources available to them are relatively limited, making them more reliant on TESS to support post-disaster recovery.

To select critical buses located at the end of formed microgrids under fault conditions as TESS stations, the consideration include evaluating the load demands of these buses under normal conditions, as shown by the blue bars

Table 5: Simulation results of the effects of TESS under different scenarios.

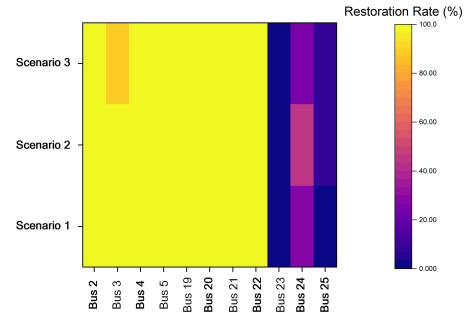
Scenario TESS	Scenario 1		Scenario 2		Scenario 3	
	Without TESS	TESS	Without TESS	TESS	Without TESS	TESS
Total Cost (\$)	8324.69	3355.17 (59.7% ↓)	11810.64	7572.59 (35.89% ↓)	23720.33	21667.39 (8.65% ↓)
Critical Load Restoration (%)	72.12	88.32 (16.2% ↑)	80.19	87.89 (7.7% ↑)	71.04	77.03 (5.99% ↑)
Normal Load Restoration (%)	93.08	95.97 (2.89% ↑)	85.01	75.26 (9.75% ↓)	88.83	76.67 (12.16% ↓)
Total Load Restoration (%)	79.16	90.89 (11.73% ↑)	81.86	83.52 (1.66% ↑)	75.89	76.93 (1.04% ↑)

in Fig 11, and examining the topologies of the formed microgrids, as illustrated in Fig 9. Notably, Bus 25 and Bus 14 stand out as the two primary candidates where TESS support is essential. This preference is rooted in their placement at the terminus of the microgrids, coupled with relatively high energy demands across all three scenarios. Considering the transportation network and the long distance between these two buses located at the end of the microgrids, it is unnecessary to designate both of them as TESS stations. This is due to the excessive time needed to move TESS between these two buses. Therefore, based on the above analysis, there are two possible optional groups of stations for TESS to choose from: (Bus 25, Bus 4, Bus 26) and (Bus 14, Bus 4, Bus 26). The post-disaster restoration effects with the two different options of TESS stations are illustrated in Table 4. It should be noted that, due to the larger capacity of the wind turbine generator at Bus 26, TESS can have a greater flexibility in scheduling at this bus after a HILP event occurs. Therefore, among all station combinations, Bus 26 is chosen as the initial location for TESS.

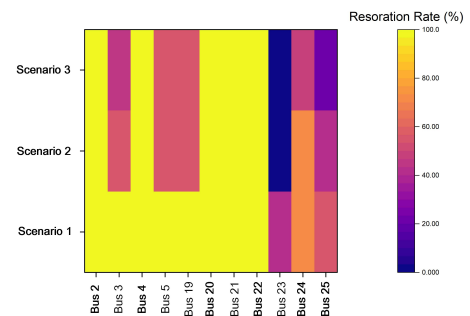
As listed in Table 4, when Bus 25, Bus 26 and Bus 4 are selected as the TESS stations, the overall post-disaster restoration costs across all three fault scenarios are lower than the other substation group. Further, as shown in Fig 11, in all the fault scenarios, Bus 25 is always the weakest bus, and in scenario 1, the restoration rate of Bus 25 is even zero without the assistance of TESS. Therefore, Bus 25 requires the most TESS support, confirming that choosing Bus 25 as a TESS station is preferable to selecting Bus 14. In summary, (Bus 25, Bus 4, Bus 26) is the optimal station group for handling all the fault scenarios in the case study. It is worth noting that the selection of TESS stations should be based on the fault conditions. Different fault scenarios may result in distinct microgrid topologies, leading to different station selection options.

4.3.2. The effects and behavior analysis of TESS

Table 5 lists the economic costs and the load restoration rates with and without TESS under different scenarios. As shown in this table, the economic costs with TESS are clearly reduced, with a maximum reduction of 59.7%. Besides, the critical load restoration rates are improved, with improvement ranging from 5.99% to 16.2%. On the contrary, the normal load restoration rates in Scenario 2



(a) Load restoration without TESS in **Area 1**



(b) Load restoration with TESS in **Area 1**

Figure 12: The impact of TESS on the loads restoration in **Area 1**.

and Scenario 3 are reduced by 9.75% and 12.16% respectively. The impact of TESS on post-disaster load restoration in **Area 1** is illustrated in Fig 12. As shown in this figure, the bus in bold face indicates that the load connected to this bus is critical. As shown from the comparison of Fig 12 (a) and 12 (b), TESS enables the microgrid in **Area 1** to provide more power to critical loads during the post-disaster recovery period, thus improve the restoration rates of these critical loads.

While TESS helps the distribution network recover from the fault scenarios under investigation, their charging or discharging arrangement according to the proposed restoration scheme is illustrated in Fig 13. As shown in Fig 13, in all three scenarios, TESS will first release its power at Bus 26, and then move to Bus 25 to charge until reaching its maximum capacity. The result presented in Fig 13 also reflect the travel distances between the three stations in the transportation network. As shown in the traffic net-

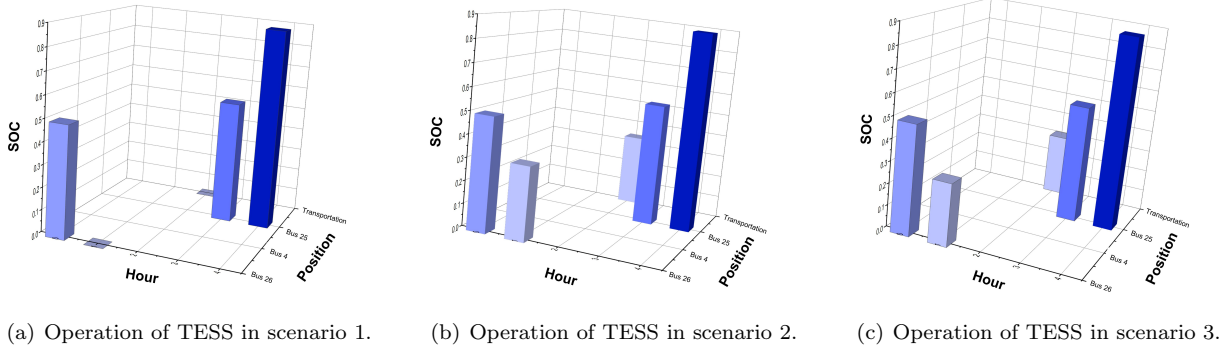
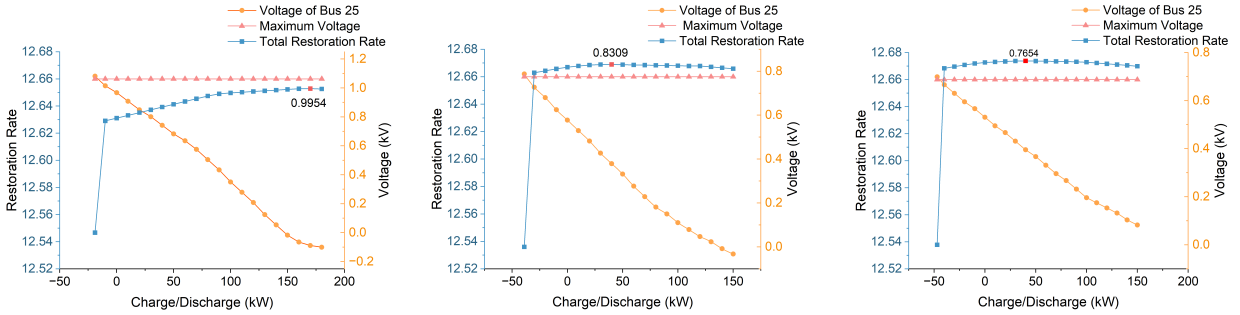


Figure 13: Operation of TESS under different scenarios.



(a) TESS behavior analysis in scenario 1. (b) TESS behavior analysis in scenario 2. (c) TESS behavior analysis in scenario 3.

Figure 14: Behavior analysis for TESS under different scenarios.

work in Fig 5, the distance from Bus 4 to Bus 26 is greater than the distances between other TESS stations. If TESS chooses to move between these two stations, it implies a longer transportation time which does not effectively contribute to the post-disaster recovery. Additionally, it is commonly understood that if a load has a low restoration rate during the post-disaster recovery, TESS should be arranged to discharge to satisfy this load to help improve the restoration rate. But this study reveals that if TESS is arranged to discharge Bus 25 directly, the total critical load restoration rate would decrease and even the entire microgrid may collapse, this situation can be illustrated in Fig 14.

As shown in Fig 14, in this experiment, Bus 25 is assumed to be connected with a stationary energy storage system (SESS), which charges or discharges Bus 25 in equal amount each hour during the post-disaster recovery stage. If the SESS is arranged to discharge at Bus 25, the voltage of Bus 25 will increase accordingly, and when the voltage of Bus 25 exceeds the maximum voltage limit, the microgrid would collapse. In contrast, if a suitable charging scheme of the SESS is applied to Bus 25, the highest load restoration rate can be achieved. TESS here plays the role of balancing voltage constraints for Bus 25, where TESS is first scheduled to discharge at Bus 26 and then move to Bus 25 for charging, which can help improve the restoration rates of the critical loads and reduce the interruption costs effectively while satisfying the constraints of the power system.

4.4. The effect analysis of the proposed restoration scheme

4.4.1. Effects on the modified IEEE 33-bus system

Table 6 presents a comparison of the proposed restoration scheme based on TESS and SOP with the traditional tie switch-based restoration scheme. It is shown that in Scenario 1, the effects are the most obvious, with the total cost reduction by 81.7% and the total load restoration rate improvement by 48.36%. Furthermore, as the results presented in Table 6 indicate, the restoration rate of critical loads is consistently higher than that of normal loads in all three scenarios. Since the interruption costs of critical loads are obviously higher than those of normal loads, it is necessary to shed some normal loads to improve the restoration rates of the critical loads, and thus reduce the economic costs during the post-disaster recovery.

Table 7 lists a comparison of the restoration rates for different types of normal loads under various scenarios. It should be noted that, due to voltage constraints influenced by TESS, the results presented here do not include Bus 23. From this table, it can be observed that the proposed restoration scheme consistently prioritizes the restoration of industrial loads when it comes to normal load restoration. This disparity is attributed to the difference of the interruption costs for different normal load types, where the interruption cost for industrial normal loads is the highest. Therefore, prioritizing the restoration of industrial normal loads can further reduce the interruption costs.

In short, the proposed restoration scheme is capable of identifying the solution with the lowest interruption cost

Table 6: The effects of TESS and SOP under different scenarios.

Scenario	Scenario 1		Scenario 2		Scenario 3	
	Tie Switch	TESS & SOP	Tie Switch	TESS & SOP	Tie Switch	TESS & SOP
Total Cost (\$)	18420.6	3355.17 (81.7% ↓)	21928.46	7572.59 (65.47% ↓)	49307.94	21667.39 (56.06% ↓)
Critical Load Restoration (%)	45.43	88.32 (42.89% ↑)	59.1	87.89 (28.79% ↑)	45.04	77.03 (31.99% ↑)
Normal Load Restoration (%)	36.80	95.97 (59.17% ↑)	53.32	75.26 (21.94% ↑)	60.16	76.67 (16.51% ↑)
Total Load Restoration (%)	42.53	90.89 (48.36% ↑)	57.1	83.52 (26.42% ↑)	49.16	76.93 (27.77% ↑)

Table 7: Comparison of the restoration rates for different types of normal loads.

	Residential Normal Load Restoration(%)	Commercial Normal Load Restoration(%)	Industrial Normal Load Restoration(%)
Scenario 1	100	100	100
Scenario 2	72.45	78.56	100
Scenario 3	69.97	96.55	100

in different fault scenarios, which not only considers the prioritized restoration of critical loads but also ranks the restoration priorities for different types of normal loads based on their interruption costs. When the power supply is limited, the proposed scheme prioritizes the restoration of critical loads and specific normal loads with relatively higher interruption costs. While normal loads with relatively lower interruption costs are prioritized for sacrifice when the energy supply is limited.

4.4.2. Effects of different scale of wind energy outputs

As a growing number of distributed renewable generating units, such as wind and solar power generators, are integrated to the power network at all voltage level, it offers more potentials to increase the power network resilience. However, due to the inherent dependence of renewable power generation on natural weather conditions, accurately predicting their power outputs poses a significant challenge. In the context of the post-disaster restoration scheme proposed in this paper, where wind power generation serves as a vital power source, the inherent uncertainty associated with wind power will undoubtedly exert a significant impact. To evaluate the adaptability of the proposed restoration scheme to the varying weather conditions, this paper employs the proposed scheme to different failure scenarios encompassing different scales of wind energy output.

In this paper, the wind power generation data is taken from Elia Grid [44]. To validate the post-disaster restoration scheme proposed in this paper under various wind power output scenarios, data from three different scales of wind power output, high, medium, and low, have been selected. Consequently, three scenarios are constructed: high-scale wind energy, medium-scale wind energy, and low-scale wind energy. In this study, the different wind power output scenarios are applied to the aforementioned three fault scenarios occurring at different time periods,

aiming to comprehensively evaluate the effectiveness of the proposed restoration scheme. The corresponding results are illustrated in Fig 15.

As shown in Fig 15, when the wind power generation is at a low scale, the proposed restoration scheme demonstrates a notable capability to efficiently restore the critical loads, and this effect is particularly evident in Scenario 2 and Scenario 3 when the load demand is at a high level. These results highlight the effects of the proposed restoration scheme to allocate the limited energy resources during the post-disaster recovery phase, particularly in situations with inadequate energy supply. By optimizing the limited energy distribution, critical loads will be prioritized for restoration, thereby reducing post-disaster restoration costs.

4.4.3. Effects on the modified IEEE 69-bus system

In order to further verify the effectiveness of the proposed post-disaster restoration scheme, the resilient operation is implemented on a modified IEEE 69-bus system, as shown in Fig 16. The initial configuration has four WTGs, 69 load buses, 68 transmission lines and 2 TESS. The line faults occur on lines (1, 2), (3, 28), (3, 28), (8, 9), (22, 23) and (60, 61). When the line faults occur, the test system loses connections from the main grid and loses the loads from Bus 61 to Bus 65. In order to reconnect these losing loads, SOP is used to connect Bus 27 and Bus 65. Subsequently, four microgrids are established, powered by four WTGs and supported by TESS, to facilitate load restoration.

In the proposed modified IEEE 69-bus system, No.1, No.2 and No.3 wind turbine generators have a rated power of 850kW each, while the No.4 wind turbine generator has a rated power of 2000kW. Regarding the selection of TESS stations, Bus 52 is chosen as a shared station for the two TESSs due to its position at the far end of the microgrid where the No.4 wind turbine generator is connected. This

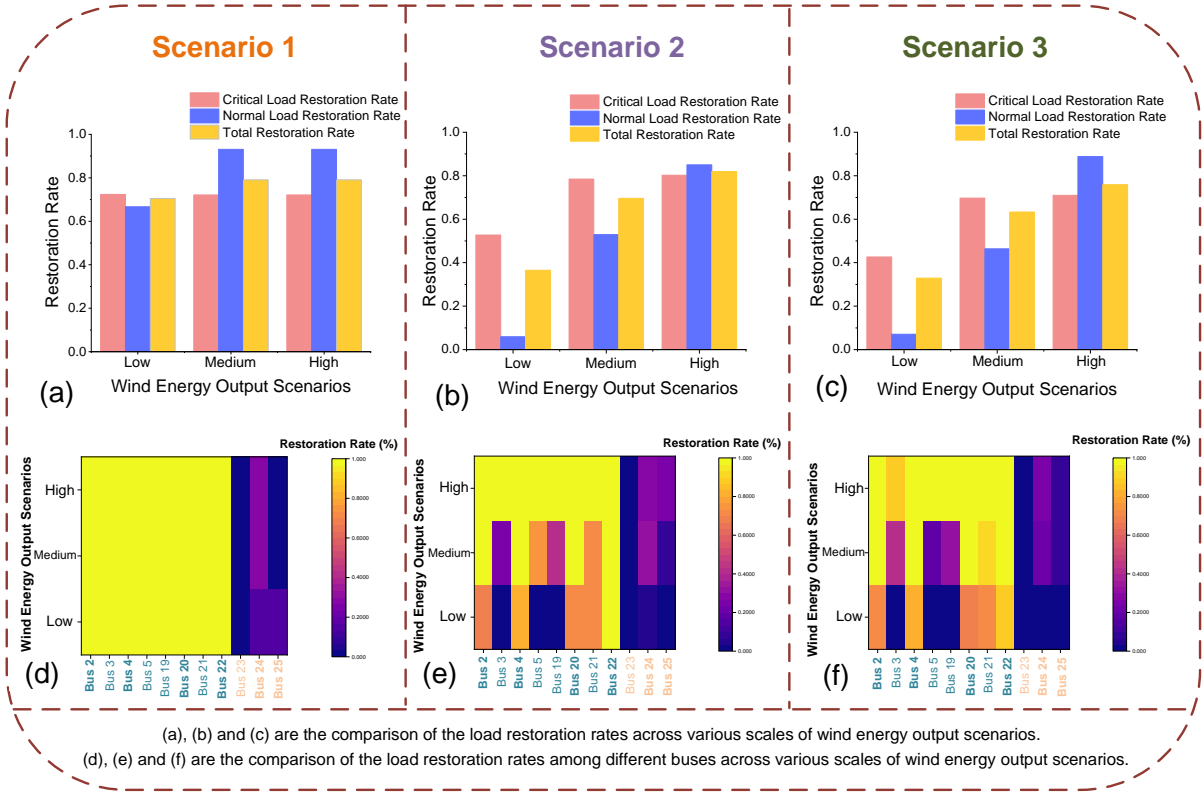


Figure 15: Effects of different scales of wind energy output on load restoration rates.

microgrid is also the largest among the four microgrids. Furthermore, Bus 23, Bus 34, Bus 44, and Bus 60 are chosen as additional stations due to their proximity to the wind turbine generators. The proposed scheme is applied to three fault scenarios occurring at different time periods, and the obtained results are presented in Fig 17.

Fig 17 (a), (b) and (c) show the wind power generation and the power demand of the test system under the three scenarios. Furthermore, several critical buses with significant load demands are selected to assess the efficacy of the proposed scheme during the post-disaster restoration phase, as shown in Fig 17 (d), (e) and (f). It is evident that, across the three scenarios, the post-disaster restoration rate of the critical loads with high demand can achieve a complete restoration (reaching 100%) with the support of TESS and SOP. Nevertheless, if the post-disaster restoration solely relies on tie switches, the restoration rate of weak nodes located at the end of the microgrid, such as Bus 49 and Bus 50, would experience a substantial decrease.

The effects of the proposed scheme on the modified 69-bus system are detailed in Table 8, highlighting the differences in comparison to the traditional tie switch scheme. In Scenario 2, aided by TESS and SOP, the recovery phase witnessed the most significant reduction in total cost, reaching 93.3%. While in Scenario 1, the critical load restoration rate shows the highest improvement, reaching 74.25%. Based on the results presented in Table 8, it is evident that the proposed scheme can yield favorable outcomes even in

larger-scale systems. This further substantiates the applicability of the proposed scheme to power systems of different scales under different fault scenarios.

5. Discussion

The future distribution system is expected to integrate more distributed renewable generators and energy storage systems. Innovative utilization of these resources can further enhance the resilience of the distribution system. In this context, this paper has designed a post-disaster restoration scheme for the distribution system integrated with wind turbine generators, SOP and TESS as its core devices. In this restoration scheme, wind turbine generators play a primary role as the main energy source for the microgrids formed during the post-disaster recovery period. SOP is responsible for adjusting the topology of the distribution system based on fault conditions, ensuring that the formed microgrids can supply the loads in the distribution system as much as possible. TESS, on the other hand, is responsible for allocating and adjusting energy resources among microgrids during the post-disaster recovery period, thereby further enhancing recovery efficiency.

This study has demonstrated that a holistic consideration of both the power network and transport network based on their couplings is essential for enhancing the overall system resilience and simultaneously reducing the costs. This is particularly relevant for future power networks

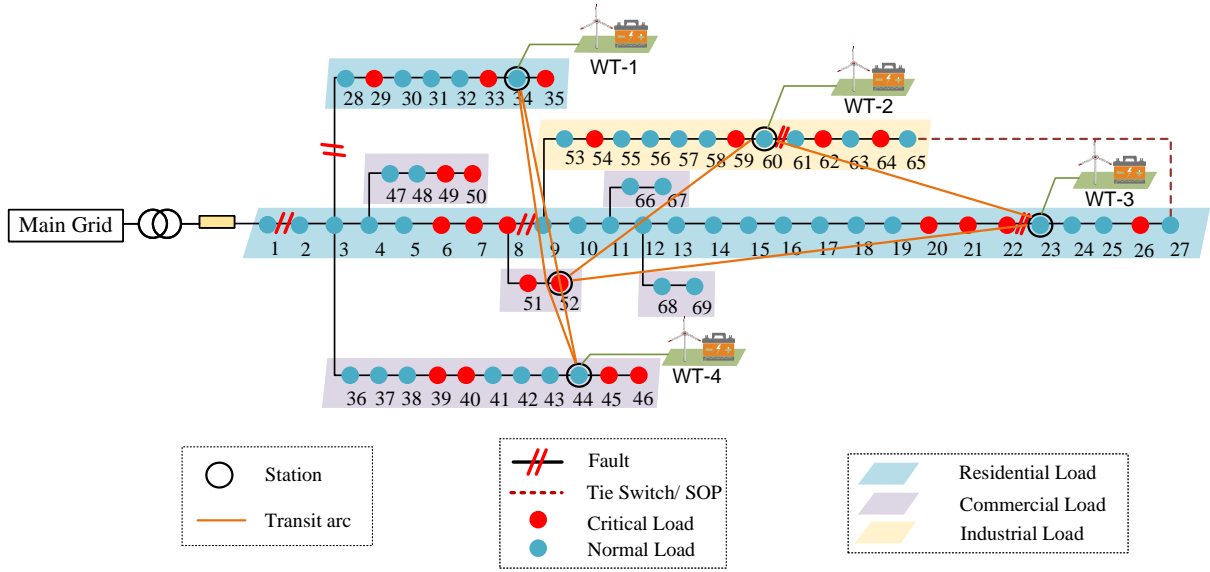


Figure 16: The modified IEEE 69-bus system diagram.

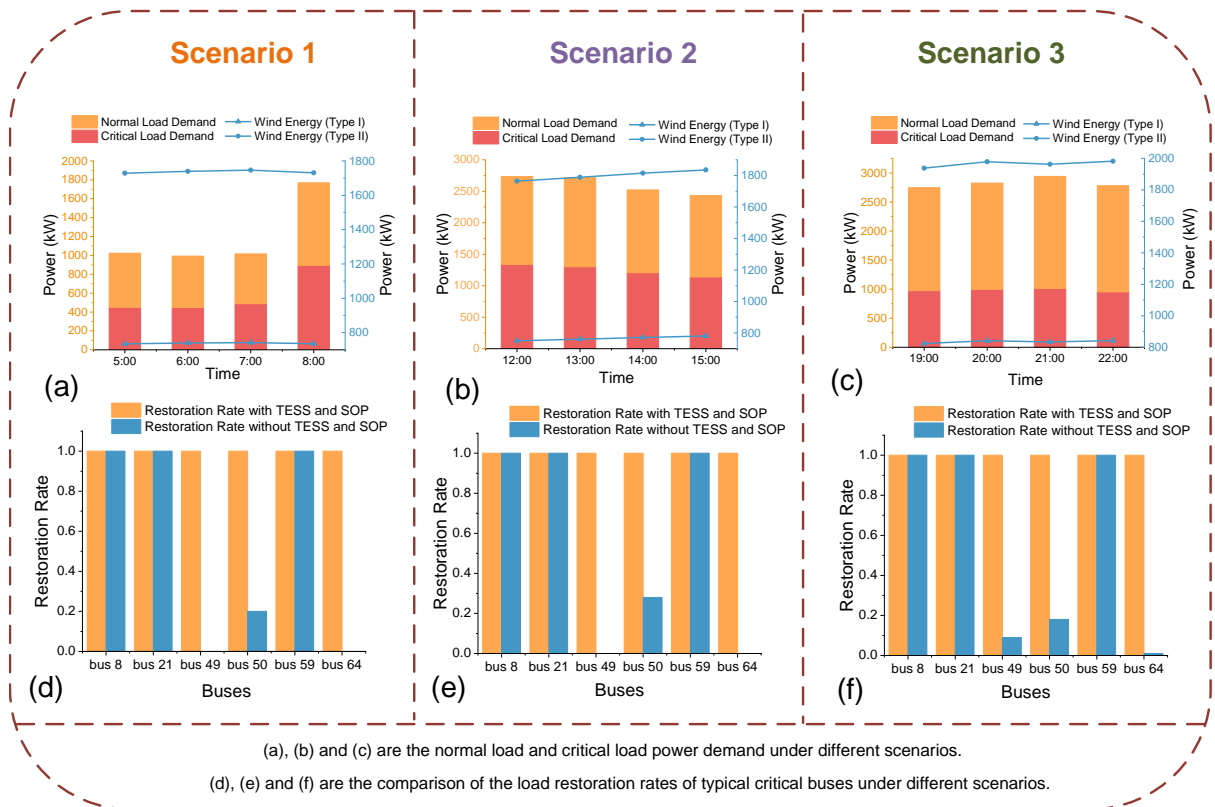


Figure 17: Fault scenarios and results analysis on the modified IEEE 69-bus system.

running on distributed renewable sources and integrated with decarbonized transport networks. A future work will consider the implementation of this proposed framework in real applications, where the models will become much more complicated, and the cost benefit analysis is also often required for engineering design and development.

6. Conclusion

In this paper, a resilient scheme of post-disaster restoration for distribution networks with WGT, SOP and TESS has been developed. This restoration scheme takes into account not only the prioritized restoration of critical loads but also the pickup of specific normal loads with high interruption costs, thereby minimizing losses during the fault period. During the post-disaster recovery phase of the

Table 8: The effects of TESS and SOP under different scenarios on the modified 69-bus system.

Scenario	Scenario 1		Scenario 2		Scenario 3	
	Tie Switch	TESS & SOP	Tie Switch	TESS & SOP	Tie Switch	TESS & SOP
Total Cost (\$)	21911.45	1510.69	40830.02	2735.69 (93.3% ↓)	29840.5	8328.93
Critical Load Restoration (%)	25.75	100 (74.25% ↑)	31.9	100	50.58	100
Normal Load Restoration (%)	32.02	87.43	41.53	68.18	32.79	43.37
Total Load Restoration (%)	29.04	93.4	36.91	83.43	39	63.15

distribution network, the appropriate topology is reconfigured firstly according to the fault scenarios aided with WTG and SOP, and the microgrids are formed accordingly to restore the disconnected loads. In addition, the stations of TESS are selected according to the fault scenarios and the formed microgrids. Afterwards, TESS are managed to charge or discharge at these stations to support load restoration. To evaluate the effectiveness of the post-disaster restoration scheme, a cost model for the post-disaster restoration period has also been formulated.

In order to verify the general applicability of the proposed post-disaster restoration scheme, a number of fault scenarios occurring at different times of a day and with different scales of wind power generations are investigated. Experimental results confirm that the proposed post-disaster restoration scheme could effectively improve the loads restoration rates of distribution network during the post-disaster restoration, especially the critical loads and specific normal load types with relatively high restoration costs. The achieved results demonstrate an impressive up to 93.3% reduction in recovery costs and a notable up to 74.25% increase in the restoration rate of critical loads. In addition, impacts of TESS during the post-disaster recovery of the distribution network are analyzed in details, and the results confirm that TESS can play an important role in restoring the critical loads while satisfying the constraints of the power system.

Acknowledgments

Shihao Zhao would like to thank the China Scholarship Council for the financial support of his PhD study at University of Leeds. This work is partially supported by the Ofgem/UKRI SIF project 'Resilient and Flexible Railway Multi-Energy Hub Networks for Integrated Green Mobility', SP Energy Network Funded project 'A holistic approach for power system monitoring to support DSO transition'.

References

- [1] Wang, C., Ju, P., Wu, F., Pan, X., Wang, Z.: A systematic review on power system resilience from the perspective of generation, network, and load. *Renewable and Sustainable Energy Reviews* **167** (2022) 112567
- [2] Li, X., Du, X., Jiang, T., Zhang, R., Chen, H.: Coordinating multi-energy to improve urban integrated energy system resilience against extreme weather events. *Applied Energy* **309** (2022) 118455
- [3] Younesi, A., Shayeghi, H., Wang, Z., Siano, P., Mehrizi-Sani, A., Safari, A.: Trends in modern power systems resilience: State-of-the-art review. *Renewable and Sustainable Energy Reviews* **162** (2022) 112397
- [4] Force, G.R.T.: Weathering the storm: report of the grid resiliency task force. Maryland Energy Administration, Baltimore, Maryland, USA.[online] URL: https://www.bateswhite.com/media/publication/13_GridResiliencyTaskForceReport.pdf (2012)
- [5] Jesse, B.J., Heinrichs, H.U., Kuckshinrichs, W.: Adapting the theory of resilience to energy systems: a review and outlook. *Energy, Sustainability and Society* **9**(1) (2019) 1–19
- [6] Saravi, V.S., Kalantar, M., Anvari-Moghaddam, A.: Resilience-constrained expansion planning of integrated power–gas–heat distribution networks. *Applied Energy* **323** (2022) 119315
- [7] Zhang, D., Li, C., Goh, H.H., Ahmad, T., Zhu, H., Liu, H., Wu, T.: A comprehensive overview of modeling approaches and optimal control strategies for cyber-physical resilience in power systems. *Renewable Energy* (2022)
- [8] Poudyal, A., Poudel, S., Dubey, A.: Risk-based active distribution system planning for resilience against extreme weather events. *IEEE Transactions on Sustainable Energy* (2022)
- [9] Gargari, M.Z., Hagh, M.T., Zadeh, S.G.: Preventive scheduling of a multi-energy microgrid with mobile energy storage to enhance the resiliency of the system. *Energy* **263** (2023) 125597
- [10] Papari, B., Edrington, C.S., Ghadamyari, M., Ansari, M., Ozkan, G., Chowdhury, B.: Metrics analysis framework of control and management system for resilient connected community microgrids. *IEEE Transactions on Sustainable Energy* **13**(2) (2021) 704–714
- [11] Kanakadhurga, D., Prabakaran, N.: Demand side management in microgrid: A critical review of key issues and recent trends. *Renewable and Sustainable Energy Reviews* **156** (2022) 111915
- [12] Mansouri, S.A., Ahmarinejad, A., Nematbakhsh, E., Javadi, M.S., Nezhad, A.E., Catalão, J.P.: A sustainable framework for multi-microgrids energy management in automated distribution network by considering smart homes and high penetration of renewable energy resources. *Energy* **245** (2022) 123228
- [13] Hussain, A., Bui, V.H., Kim, H.M.: Microgrids as a resilience resource and strategies used by microgrids for enhancing resilience. *Applied Energy* **240** (2019) 56–72
- [14] Chen, C., Wang, J., Qiu, F., Zhao, D.: Resilient distribution system by microgrids formation after natural disasters. *IEEE Transactions on Smart Grid* **7**(2) (2015) 958–966
- [15] Fu, W., Xie, H., Zhu, H., Wang, H., Jiang, L., Chen, C., Bie, Z.: Coordinated post-disaster restoration for resilient urban distribution systems: A hybrid quantum-classical approach. *Energy* **284** (2023) 129314
- [16] Huang, Y., Li, G., Chen, C., Bian, Y., Qian, T., Bie, Z.: Resilient distribution networks by microgrid formation using deep reinforcement learning. *IEEE Transactions on Smart Grid* **13**(6) (2022) 4918–4930
- [17] Khaledi, A., Saifoddin, A.: Three-stage resilience-oriented ac-

- tive distribution systems operation after natural disasters. *Energy* **282** (2023) 128360
- [18] Borghei, M., Ghassemi, M.: Optimal planning of microgrids for resilient distribution networks. *International Journal of Electrical Power & Energy Systems* **128** (2021) 106682
- [19] Zhao, S., Li, K., Yang, Z., Xu, X., Zhang, N.: A new power system active rescheduling method considering the dispatchable plug-in electric vehicles and intermittent renewable energies. *Applied Energy* **314** (2022) 118715
- [20] Li, Y., Sun, Y., Liu, J., Liu, C., Zhang, F.: A data driven robust optimization model for scheduling near-zero carbon emission power plant considering the wind power output uncertainties and electricity-carbon market. *Energy* (2023) 128053
- [21] Zhu, X., Zhao, S., Yang, Z., Zhang, N., Xu, X.: A parallel meta-heuristic method for solving large scale unit commitment considering the integration of new energy sectors. *Energy* **238** (2022) 121829
- [22] Nikkhah, S., Jalilpoor, K., Kianmehr, E., Gharehpetian, G.B.: Optimal wind turbine allocation and network reconfiguration for enhancing resiliency of system after major faults caused by natural disaster considering uncertainty. *IET Renewable Power Generation* **12**(12) (2018) 1413–1423
- [23] Nikoobakht, A., Aghaei, J.: Resilience promotion of active distribution grids under high penetration of renewables using flexible controllers. *Energy* **257** (2022) 124754
- [24] Wang, Z., Wang, J.: Self-healing resilient distribution systems based on sectionalization into microgrids. *IEEE Transactions on Power Systems* **30**(6) (2015) 3139–3149
- [25] Krishnamurthy, V., Kwasinski, A.: Effects of power electronics, energy storage, power distribution architecture, and lifeline dependencies on microgrid resiliency during extreme events. *IEEE Journal of Emerging and Selected Topics in Power Electronics* **4**(4) (2016) 1310–1323
- [26] Chi, Y., Xu, Y., Ding, T.: Coordinated var planning for voltage stability enhancement of a wind-energy power system considering multiple resilience indices. *IEEE Transactions on Sustainable Energy* **11**(4) (2019) 2367–2379
- [27] Gilani, M.A., Kazemi, A., Ghasemi, M.: Distribution system resilience enhancement by microgrid formation considering distributed energy resources. *Energy* **191** (2020) 116442
- [28] Saboori, H., Jadid, S.: Optimal scheduling of mobile utility-scale battery energy storage systems in electric power distribution networks. *Journal of Energy Storage* **31** (2020) 101615
- [29] Sun, Y., Zhong, J., Li, Z., Tian, W., Shahidehpour, M.: Stochastic scheduling of battery-based energy storage transportation system with the penetration of wind power. *IEEE Transactions on Sustainable Energy* **8**(1) (2016) 135–144
- [30] Shen, Y., Qian, T., Li, W., Zhao, W., Tang, W., Chen, X., Yu, Z.: Mobile energy storage systems with spatial-temporal flexibility for post-disaster recovery of power distribution systems: A bilevel optimization approach. *Energy* **282** (2023) 128300
- [31] Yao, S., Wang, P., Zhao, T.: Transportable energy storage for more resilient distribution systems with multiple microgrids. *IEEE Transactions on Smart Grid* **10**(3) (2018) 3331–3341
- [32] Dabbaghjamanesh, M., Senemmar, S., Zhang, J.: Resilient distribution networks considering mobile marine microgrids: A synergistic network approach. *IEEE Transactions on Industrial Informatics* **17**(8) (2020) 5742–5750
- [33] Kim, J., Dvorkin, Y.: Enhancing distribution system resilience with mobile energy storage and microgrids. *IEEE Transactions on Smart Grid* **10**(5) (2018) 4996–5006
- [34] Liang, X., Saaklayen, M.A., Igder, M.A., Shawon, S.M.R.H., Faried, S.O., Janbakhsh, M.: Planning and service restoration through microgrid formation and soft open points for distribution network modernization: a review. *IEEE Transactions on Industry Applications* (2022)
- [35] Lv, C., Liang, R., Zhang, G., Zhang, X., Jin, W.: Energy accommodation-oriented interaction of active distribution network and central energy station considering soft open points. *Energy* **268** (2023) 126574
- [36] Cao, W., Wu, J., Jenkins, N., Wang, C., Green, T.: Benefits analysis of soft open points for electrical distribution network operation. *Applied Energy* **165** (2016) 36–47
- [37] Ding, T., Wang, Z., Jia, W., Chen, B., Chen, C., Shahidehpour, M.: Multiperiod distribution system restoration with routing repair crews, mobile electric vehicles, and soft-open-point networked microgrids. *IEEE Transactions on Smart Grid* **11**(6) (2020) 4795–4808
- [38] Li, P., Ji, J., Ji, H., Song, G., Wang, C., Wu, J.: Self-healing oriented supply restoration method based on the coordination of multiple sops in active distribution networks. *Energy* **195** (2020) 116968
- [39] Cao, W., Wu, J., Jenkins, N., Wang, C., Green, T.: Operating principle of soft open points for electrical distribution network operation. *Applied Energy* **164** (2016) 245–257
- [40] Saboori, H., Jadid, S.: Mobile and self-powered battery energy storage system in distribution networks—modeling, operation optimization, and comparison with stationary counterpart. *Journal of Energy Storage* **42** (2021) 103068
- [41] Kliewer, N., Mellouli, T., Suhl, L.: A time-space network based exact optimization model for multi-depot bus scheduling. *European Journal of Operational Research* **175**(3) (2006) 1616–1627
- [42] Zakariazadeh, A., Jadid, S., Siano, P.: Smart microgrid energy and reserve scheduling with demand response using stochastic optimization. *International Journal of Electrical Power & Energy Systems* **63** (2014) 523–533
- [43] Li, Z., Tang, W., Lian, X., Chen, X., Zhang, W., Qian, T.: A resilience-oriented two-stage recovery method for power distribution system considering transportation network. *International Journal of Electrical Power & Energy Systems* **135** (2022) 107497
- [44] Elia Group: Grid data overview (<https://www.elia.be/en/grid-data>)